J Appl Electrochem (2009) 39:411–419
DOI 10.1007/s10800-008-9686-0

ORIGINAL PAPER

Effect of support conductivity of catalytic powder on electrocatalytic hydrogenation of phenol

Dihourahouni Tountian · Anne Brisach-Wittmeyer · Paul Nkeng · Gérard Poillerat · Hugues Ménard

Received: 16 January 2008 / Accepted: 6 October 2008 / Published online: 29 October 2008

Abstract Metallic nanoaggregates deposited on non-conductive oxides powders as catalysts have shown good efficiency in electrocatalytic hydrogenation (ECH). In this process, the polarization of the metallic nanoaggregates is very important. This polarization can be improved when the electrode material is conductive. Thus, the goal of this work was to study the effect of the conduction of the supported material on the ECH process. Tin dioxide was chosen as oxide because it can be obtained in non-conductive or conductive form by doping with fluorine. Palladium supported catalysts powders were prepared by the sol–gel method. These electrocatalysts were characterized by XRD, SEM, TGA/DSC, FTIR and electrical conductivity. The effects of temperature and time of calcination were also investigated. Comparison of non-conductive and conductive catalysts for ECH of phenol shows that conductive F-doped SnO_2 increases the rate of electrohydrogenation.

Keywords Electrocatalytic hydrogenation (ECH) · Conductive catalyst supporting powder · Tin dioxide catalyst · Isotherm adsorption · Phenol

D. Tountian · P. Nkeng · G. Poillerat
Laboratoire d'Electrochimie et de Chimie Physique du Corps Solide, Institut de Chimie, UMR 7177 CNRS, Université Louis Pasteur, 4 rue Blaise Pascal, 67000 Strasbourg, France

D. Tountian · A. Brisach-Wittmeyer (✉) · H. Ménard
Laboratoire Sciences de Matériaux d'Electrodes, Département de Chimie, Université de Sherbrooke, 2500 boul. de l'Université, Sherbrooke, QC, Canada J1K2R1
e-mail: Anne.Wittmeyer@USherbrooke.ca

1 Introduction

The hydrogenation of organic compounds is an important industrial process particularly for pharmaceutical and environmental applications [1, 2]. Thus catalytic hydrogenation (CH) and electrocatalytic hydrogenation (ECH) have been developed. ECH of organic molecules is of interest to industry in the context of green chemistry [3, 4].

The effectiveness of ECH is strongly linked to the nature of the electrode materials and their adsorption properties. ECH is a process where chemisorbed hydrogen is generated by electroreduction of water to react with the species in the bulk. In this process the support was initially used to increase surface area [5]. However, recent findings indicate that the final results of ECH depend upon the nature of the support and the metal [6]. Therefore, more emphasis is placed on improving the nature of the building material of the electrodes in order to increase ECH efficiency. A variety of materials have been developed; including: Raney Ni/Ni, Raney Ni/Hg pool, Pt/Pt, Pt/C, Rh/C [7], Pt/Pt and Pt/C with different concentrations of Pt [8]; different types of composite materials incorporated in reticulated vitreous carbon (RVC) like fractal nickel (Ni), crystalline nickel boride (Ni_2B), and metallic nanoaggregates deposited on non-conductive powders like alumina, aluminum hydroxide, barium carbonate, and barium sulphate [9–11].

All these electrode materials were developed in order to control the crucial different steps involved in the mechanism of the ECH. The steps include the production of chemisorbed hydrogen (reaction 1), adsorption of the unsaturated organic molecule (reaction 2) and desorption of the hydrogenated molecule (reaction 4), as illustrated below.

$$H_3O^+ + e + M \leftrightarrow MH_{ads} + H_2O \text{ Volmer reaction} \quad (1)$$

$$Y = Z + A \leftrightarrow (Y = Z)_{ads}A \text{ adsorption} \quad (2)$$

$$(Y = Z)_{ads}A + 2MH_{ads} \leftrightarrow (YH - ZH)_{ads}A + 2M \text{ hydrogenation reaction} \quad (3)$$

$$(YH - ZH)_{ads}A \leftrightarrow YH - ZH + A \text{ desorption} \quad (4)$$

$$H_3O^+ + MH_{ads} + e \leftrightarrow M + H_2 + H_2O \text{ Heyrovsky reaction} \quad (5)$$

$$2MH_{ads} \leftrightarrow 2M + H_2 \text{ Tafel reaction} \quad (6)$$

The efficiency of the ECH is related to each of these reactions which depend on the nature of the electrode material. Two distinct sites of adsorption are considered: the metallic particles (M) for the chemisorbed hydrogen and the support (A) for the unsaturated organic compounds ($Y = Z$). For the organic compounds it is important to have a good adsorption/desorption equilibrium. Too low or too strong adsorption/desorption is harmful. Competitive reactions such as production of molecular hydrogen can also take place (steps 5 or 6).

Thus, in the case of supported electrocatalysts, the matrix (inorganic powder), which supports the metallic nanoaggregates and which monitors the adsorption of unsaturated molecules, was non-conductive until now [9–11].

Phenol hydrogenation is well known in the literature [12–15]. In ECH, it was demonstrated that the use of supported metallic nanoaggregates catalysts enhanced the process. We can also notice through the mechanism of ECH that the production of atomic chemisorbed hydrogen plays an important role. Because this chemisorbed hydrogen is generated on the metal particles in contact with the cathode, it would be interesting to use conductive supported powder in which all metallic particles would be polarized.

The aim of this work was to study the effect of support conductivity on ECH. The conductive catalysts were obtained from tin dioxide which is known to have good catalytic properties [16, 17]. The influence of the temperature and time of calcination on these catalysts were examined. The catalytic metal in this work was palladium.

2 Experimental

2.1 Electrocatalyst preparation

The catalytic powders composed of palladium nanoaggregates deposited on SnO_2 were prepared using a sol–gel method. Tin precursor solutions were prepared according to the procedure described by Siciliano [18]. The preparations contained tin tetrachloride, propanol and isopropanol. For the preparation of Pd-modified sols with Pd/Sn atomic ratio = 0.1, the prescribed amount of Pd $(OOCCH_3)_2$ (from Aldrich) dissolved in chloroform was used as Pd precursor. F-doped SnO_2 electrocatalysts were obtained by adding an aqueous solution of NH_4F, with F/Sn atomic ratio = 0.1. After evaporation of solvent at 120 °C in air, the gels were first dried at 200 °C for 2 h and then calcined in an electrical furnace at temperatures ranging from 200 to 600 °C.

2.2 Electrocatalyst characterisation

X-ray measurements were performed using a Siemens D 5000 polycrystalline diffractometer with Cu Kα (wavelength = 1.5406 Å) radiation. Diffractograms of powders were recorded in 2θ scan configuration, in the 10–80° 2θ range, at a fixed incident angle of 0.02°.

Differential scanning calorimetric and thermogravimetric analyses (DSC/TGA) were carried out in the 50–900 °C temperature range, with a heating rate of 5 °C/min in dynamic air using a TGA 92 SETARAM.

The specific surface areas of the powders were observed by the BET method on Carlo Erba Strumentazione SORPTY 1750.

Scanning electronic microscopy (SEM) of the Pd catalysts supported on tin dioxide powders was recorded using a S-4700 model HITACHI miscrocope. Particle size was estimated using this technique. FTIR transmission spectra were recorded on a Bruker IFS 25. The samples were dispersed in a KBr matrix and pressed in self-supporting disks.

The electrical resistances of powders were measured under uniaxial pressure (5,000 psi) at room temperature by introducing 1 g of sample in a mold press. The resistance value was recorded with a multi-ohmmeter.

Measurements of adsorption isotherms were carried out as described below. Cylindrical vials (25 mL) were thoroughly cleaned, rinsed with high purity water (from a Milli-Q unit) and dried. SnO_2 catalyst (0.5 g) was added to each vial, except to the vials serving as blanks, which were treated in the same way as the others except for the addition of SnO_2 catalyst. 15 mL of phenol solutions at different concentrations, prepared in acetic acid buffer adjusted to pH 5 was added to each vial. The SnO_2-catalysts-phenol suspensions were then stirred with an orbital shaker at 320 trs/min and ambient temperature (23 ± 2 °C). Adsorption isotherms were measured after the equilibrium was reached (72 h). A 0.5 mL aliquot was withdrawn from each vial, filtered and analysed by GC chromatography to determine phenol concentration.

The rates of adsorption were determined in the same dynamic cell as used for the electrocatalytic experiments in the absence of RVC. Electrocatalyst (200 mg) was introduced to the circulating cell containing 10^{-2} M of phenol in an acetic acid buffer at pH 5. The concentration of phenol was obtained as described elsewhere by withdrawing 0.2 mL aliquots as a function of time.

Hydrogen evolution reaction was studied by linear sweep voltammetry in an acetic acid buffer of 0.5 M at pH 5 using an EG&G Princeton Applied Research potentiostat, model 273A.

A saturated calomel electrode was used as a reference electrode and the working electrode was a cylindrical piece of RVC with 200 mg of catalyst.

2.3 Electrocatalytic hydrogenation process

Electrocatalytic experiments were carried out in a dynamic cell [15] equipped with variable flow chemical pump (Fisher Scientific) connected to the cell by a PVC tube. The flow rate was maintained at 1 L/min, and the circulation of the solution was upward through the cathode. All the experiments were performed under galvanostatic conditions ($I = 20$ mA) using an Agilent galvanostat 6634B model. Cathodic and anodic compartments were filled with the same electrolyte (acetic acid buffer adjusted to pH 5 with NaOH solution (10 M)). The cathode was a cylindrical piece (diameter = 24 mm, width = 12.64 mm) of reticulated vitreous carbon (RVC, 100 pores/inch, 66 cm^2 cm^{-3}) with geometrical area = 377.21 cm^2 purchased from Electrolytica Inc.; the anode was a platinum wire with external diameter of 1 mm. The compartments were separated by a nafion 117 membrane fixed at the lower end of the anodic compartment. Prior to the ECH process, 200 mg of electrocatalyst powder was added to the electrolyte solution and 50 C were passed through the system to polarize the electrocatalyst. This quantity of charge is necessary to condition the catalyst powder by the reduction of palladium oxides and to generate adsorbed hydrogen on the palladium aggregates. After that, 1 mL of phenol (Aldrich) aqueous solution was introduced. The initial concentration of phenol in the cathodic compartment before reaction was 9.58×10^{-3} M. During the ECH process, 0.5 mL aliquots were withdrawn from the catholyte and saturated with NaCl, extracted with 1 mL of chloroform, dried over sodium sulfate, and filtered. An internal standard solution (50 μL of 3.15 mg mL^{-1} of 3-methylcyclohexanol solution) was added to obtain a final volume of 450 μL of organic phase. 1 μL of this sample was injected into a gas chromatograph. The gas chromatographic analyses were carried out using a Thermo Fisher scientific Focus GC chromatograph with a flame ionisation detector (FID) and Thermo TR-5MS capillary column (30 m × 0.25 mm × 0.25 μm).

3 Results

3.1 XRD measurements

The catalysts were calcined at three different temperatures: 350, 400 and 600 °C. They were analyzed by XRD to point out the structural evolution as a function of temperature (Fig. 1). At these calcination temperatures, the diffractograms showed the characteristic peaks of SnO_2 oxide, cassiterite structure. The peaks became better defined and sharper with increasing temperature. The presence of dopant did not modify the cassiterite structure when compared the samples obtained at 400 °C. The same behaviour was observed by Esteves in fluorine doping [19].

In the case of palladium, the diffractograms revealed that the structure was linked to the temperature. At 350 °C the catalyst showed a wide peak of palladium (111) at $2\theta = 40.1$, of palladium (200) at $2\theta = 46.6$ and of palladium (220) at and $2\theta = 68.1$. These values indicated the presence of only metal palladium particles. At 400 °C, the diffractogram indicated a prevalently palladium oxide structure with peak positions at 33.89°, 41.95°, 60.21°, 71.48°, and additional peaks with weak intensity related to metal palladium. Upon increasing the temperature to 600 °C, the peaks of palladium oxide decreased in intensity and were simultaneously replaced by metallic palladium peaks.

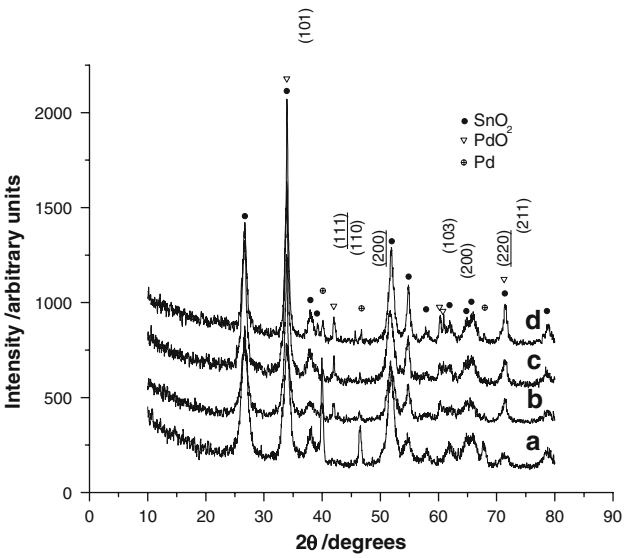

Fig. 1 X-ray diffraction pattern of (**a**) Pd/F-doped SnO_2 350 °C, (**b**) Pd/undoped SnO_2 400 °C, (**c**) Pd/F-doped SnO_2 400 °C and (**d**) Pd/F-doped SnO_2 600 °C

3.2 Thermogravimetry measurements

To understand the temperature induced changes in the palladium structure, palladium acetate powder which was the metallic precursor, was subjected to thermogravimetric analyses in the temperature range from 50 to 900 °C (Fig. 2). First, dramatic weight loss beginning at about 200 °C and ending at about 250 °C, was assigned to the pyrrolysis of organic derivatives from the powder. A corresponding exothermic phenomenon was attributed to the formation of reduced metal Pd particles. The same observation was reported by Mahfouz et al [20]. Rella et al [21] attributed this phenomenon to the spontaneous reduction of Pd to form nano-sized metal clusters.

From 350 to 550 °C the significant increase in weight was due to the oxidation of metallic palladium to palladium oxide. The second decrease in weight, with corresponding endothermic phenomenon, occurred at around 800 °C and was attributed to the reduction of palladium oxide. These observations are in agreement with reports showing that in air, at atmospheric pressure, the stable phase is PdO at temperatures below 800 °C and metallic Pd above 800 °C [22].

Thermogravimetric (DSC/TGA) analyses were also carried out in the 50–900 °C temperature range on a xerogel of F-doped SnO_2 obtained after drying at 200 °C (Fig. 3). The TG curve showed a dramatic mass loss from 158 to 300 °C, whereas the corresponding DSC curve showed an endothermic region attributed to the pyrrolysis of the organic derivatives. From 300 to about 400 °C, the weak mass loss was certainly due to the complete elimination of the organic compounds. Siciliano [18], under quasi identical conditions, made a similar observation for pure SnO_2 and found that the elimination of organic compounds was complete at 350 °C. From 400 to 460 °C an important mass loss was observed, that was attributed to the desorption of chemically bonded hydroxyl groups or to the complete disappearance of water, as observed by Zhang et al. [23] when they used tetrachloride and ethylene glycol to prepare SnO_2. Above 460 °C, no change in the TGA curve was observed, while the crystallization of F-doped tin dioxide continued, as shown by the DSC curve.

3.3 FTIR measurements

The IR spectra of the catalysts are shown in Fig. 4. Depending on temperature, different bands were observed. From 350 to 600 °C, the characteristic band of SnO_2 was seen at around 610 cm^{-1}. This band corresponds to the antisymetric Sn–O–Sn stretching mode. At 350 °C, the bands around 2,926 cm^{-1} demonstrated the presence of residual organic compounds in the powder; however, heating at 400 °C caused complete removal of the organics. At 350 and 400 °C, the presence of a broad band from 3,000 to 3,600 cm^{-1} due to the O–H stretching, and another at about 1,600 cm^{-1} associated with H–O–H in-plane deformation confirmed the DSC/TG analyses. Heating at 600 °C resulted in the disappearance of the characteristic hydroxyl and water bands.

3.4 MEB and BET measurements

As shown by the micrographs in Fig. 5, the morphology of the catalysts was strongly modified by increasing the temperature of calcination. The average particle size

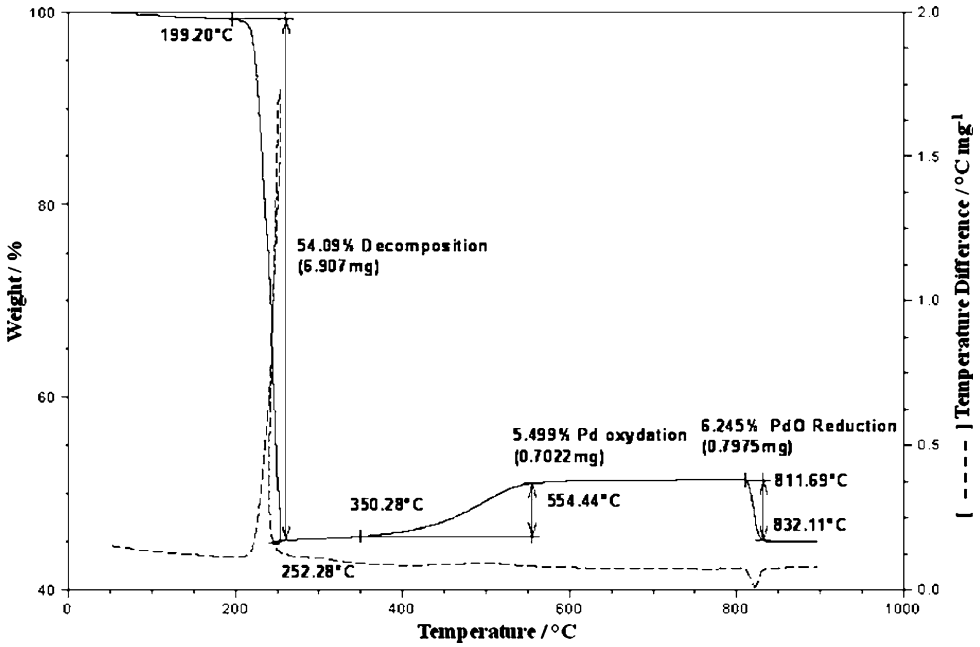

Fig. 2 TGA (—) and DSC (- - -) curves for palladium acetate powder; air atmosphere and 5 °C min^{-1} heating rate

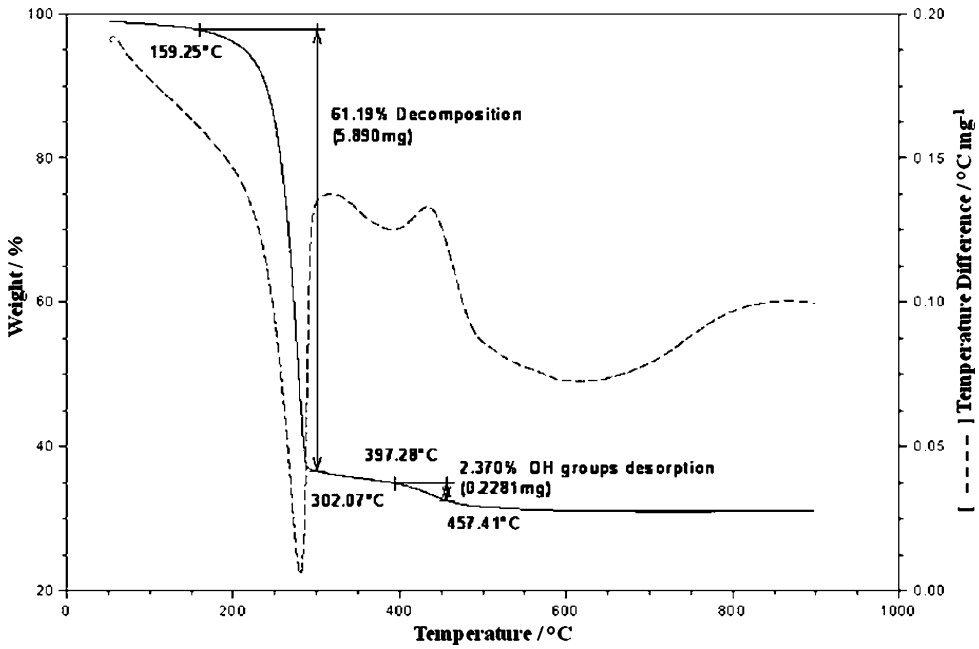

Fig. 3 TGA (—) and DSC (- - -) curves for F-doped tin oxide xerogel obtained after evaporated the solvent at 200 °C; air atmosphere and 5 °C min^{-1} heating rate

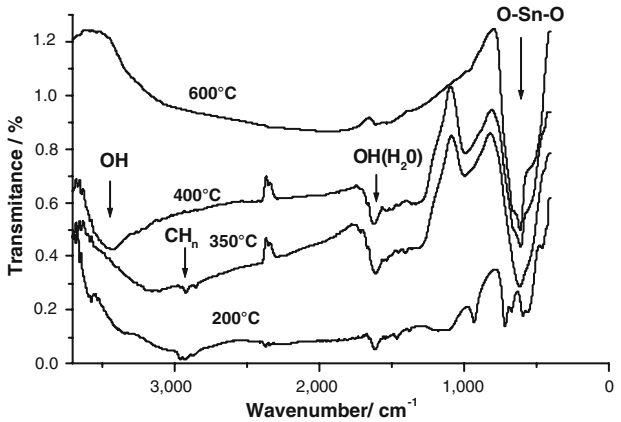

Fig. 4 FTIR spectra of Pd/F-doped SnO_2 powder at different heating temperatures

increased with heating and inversely the specific area decreased. The differences at 600 °C are the most notable. In particular, the specific area is four times smaller at 600 °C than at 350 and 400 °C (Table 1).

The cartography of these images, not presented, showed a good distribution of the different elements (Sn and O) and a uniform dispersion of metallic aggregates (Pd).

3.5 Resistivity measurements

Apart from the change of the chemical structure with the temperature, modifications of the morphology could also contribute to electrical conductivity changes. Indeed, the samples showed large fluctuations in resistivity as a function of temperature. Table 1 indicates that the resistivity decreased with annealing temperature. If at 350 °C, the samples are all non-conductors, at 400 and 600 °C they show good conduction properties. We think that the non-conduction at 350 °C was due to the presence of organic residues. Because of the presence of these residues, the sample remained non-conductor after 32 h of annealing.

The resistivity is thus influenced by the chemical composition, and also by the physical properties, principally the morphology of the powder.

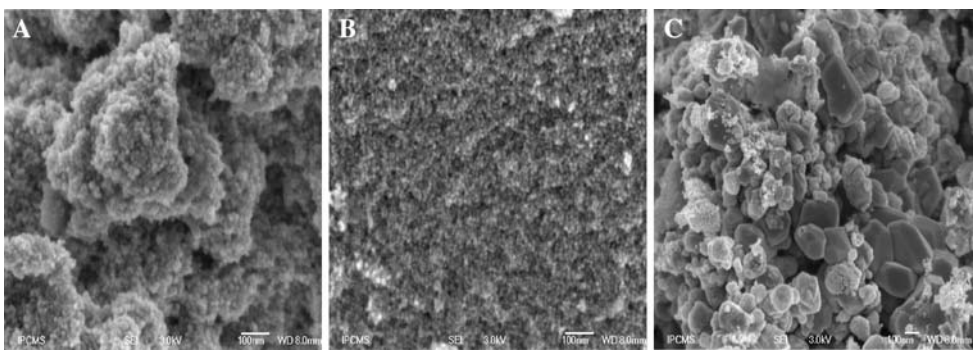

Fig. 5 SEM micrographs of Pd/F-doped SnO_2 powders calcinated during 4 hours at (**a**) 350 °C, (**b**) 400 °C and (**c**) 600 °C. *Note:* Image (**c**) is not displayed on the same scale as (**a**) and (**b**)

Table 1 Average grain size, specific area and resistivity as a function of the electrocatalyst and the heating temperature

Electrocatalyst	Calcination temperature/°C (4 h)	Particules sizes/nm	Specific area/$m^2\ g^{-1}$ (±1)	Resistivity/ Ω cm
$PdSnO_2F$	350	8–10	108	$>5 \times 10^4$
$PdSnO_2$	400	–	88	6,200–6,600
$PdSnO_2F$	400	10–20	95	100–230
$PdSnO_2F$	600	100–300	24	10–90

3.6 ECH of phenol

Phenol electrohydrogenation is a two step process. First, cyclohexanone is formed, implying four hydrogen radicals and four electrons, then, cyclohexanone is reduced to cyclohexanol, implying two hydrogens and two electrons (Scheme 1).

Figure 6 presents the phenol remaining in the ECH process as a function of the total charge, with pure Pd nanoparticles powder and SnO_2 powder under identical experimental conditions. The pure nanoparticles of Pd provided 11% depletion of phenol after 400 C, whereas no depletion of phenol was observed for SnO_2 powder. For the SnO_2 powder, even if the adsorption phenomenon takes place, there is no chemisorbed hydrogen production. In the case of Pd nanoparticles, it was demonstrated by Cirtiu et al. [15] that there is a weak adsorption of phenol to combine with the chemisorbed hydrogen produced at the cathode electrode. Thus, it is important to find the best catalyst synthesis which will take into account the two parameters.

For all the catalysts, before introducing the target molecule to be hydrogenated, the electrocatalyst is added to the acetic acid buffer and conditioned by passing 50 C through the system. Figure 7 presents the X-ray patterns of the electrocatalyst before and after passing 50 C.

It appears clearly that the polarization of the electrode has a phase modifying effect on the Pd structure.

After 50 C, the diffractograms showed that fcc Pd metal peaks replaced those of PdO. The presence of metallic Pd is necessary because the production of chemisorbed hydrogen is favoured on the metallic palladium aggregates. We can also conclude from this observation that, after applying the conditioning current, only metallic Pd particles were present for all the catalysts, independent of the temperature of calcination.

To establish the effect of the support conduction, we compared the ECH process on Pd/undoped and Pd/F-doped

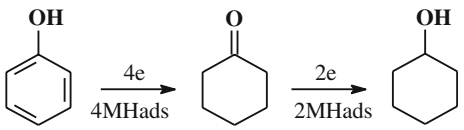

Scheme 1 Reaction scheme for phenol electrocatalytic hydrogenation

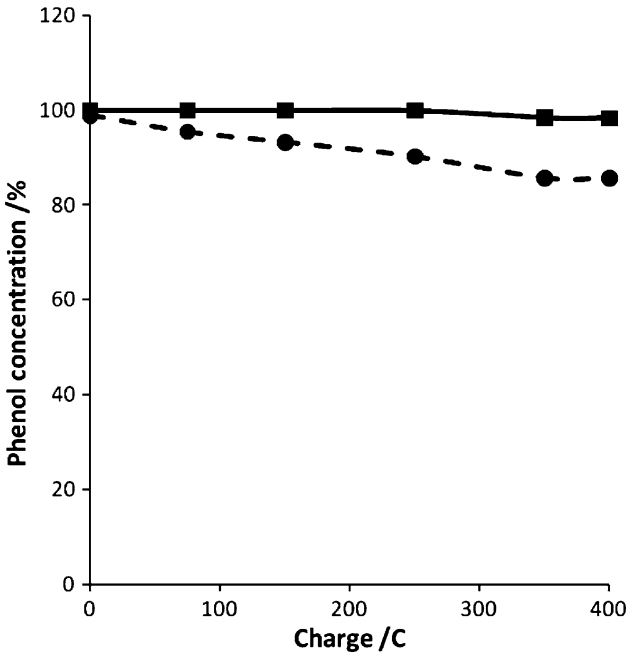

Fig. 6 Remaining fraction of phenol in acetic buffer (0.5 M) at pH 5 as a function of the total charge on SnO_2 400 °C (■) and on Pd nanoparticles (●)

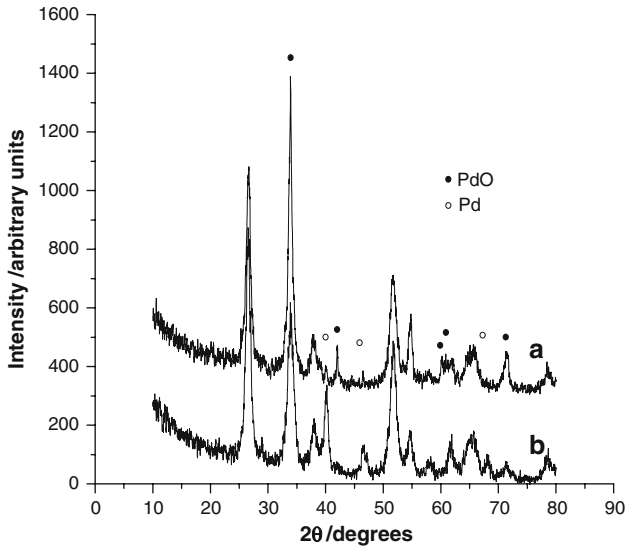

Fig. 7 X-ray diffraction pattern of (**a**) Pd/F-doped SnO_2 400 °C before and (**b**) after passed 50 C

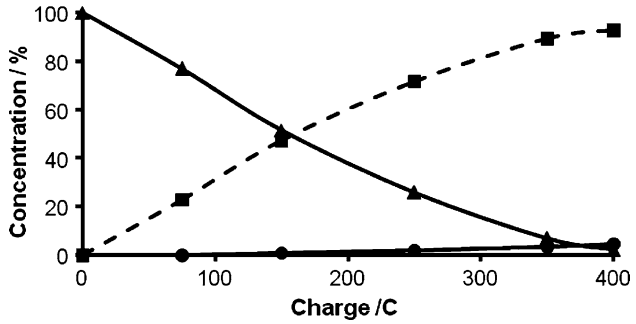

Fig. 8 ECH of phenol on Pd/undoped SnO_2 400 °C in acetic buffer 0.5 M, pH 5 as a function of the total charge: (▲) phenol, (■) cyclohexanone and (●) cyclohexanol

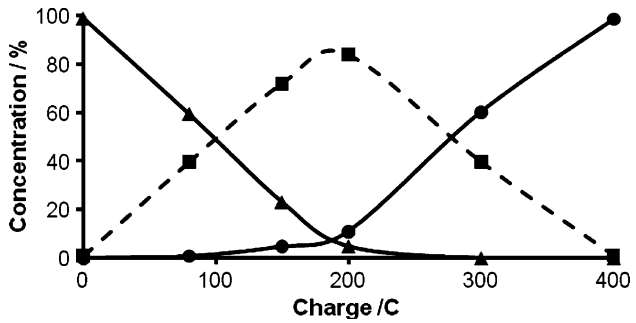

Fig. 9 ECH of phenol on Pd/F-doped SnO_2 400 °C in acetic buffer 0.5 M, pH 5 as a function of the total charge: (▲) phenol, (■) cyclohexanone and (●) cyclohexanol

SnO_2 catalyst. Figures 8 and 9 show ECH results for the two catalysts.

These results demonstrate that, (i) the support plays a key role in the ECH process because its presence at the same time as that of Pd nanoparticles causes high efficiency in hydrogenation. This efficiency is linked to the adsorption of the target molecule near the adsorbed hydrogen produced on Pd nanoparticles. These positions located at the interface between the matrix and metallic nanoparticles were called adlienation points by Maxted and Ali [24].

The adsorption is thus a crucial step in the ECH process because without matrix, the efficiency is marginal; the adsorption of the target organic occurs on the matrix. The same conclusions were pointed out by Cirtiu et al when a Pd/alumina catalyst was used (15). (ii) Undoped tin dioxide catalyst leads principally to the formation of cyclohexanone, whereas F-doped tin dioxide leads to 100% of cyclohexanol; the final product for identical corresponding charge being equal to 400 C.

4 Discussion

From all the characterizations, we can infer that the difference in ECH process between undoped and F-doped catalyst seems to be induced by the difference in the catalyst conductivities. Indeed, XRD, FTIR and thermogravimetric analyses show that the two kinds of catalysts are similar in structure and composition. However, resistivity measurements show that the doped catalyst is thirty times more conducting than the undoped one. Improving matrix conductivity contributes to a more efficient ECH process. The electrocatalytic activity of Pd/F-doped SnO_2 through RVC electrode is explained by the simultaneous polarization of all of the metallic Pd nanoaggregates present on the surface as well as in the pores of the matrix. This polarization offers a better production of chemisorbed atomic hydrogen and a large available number of adlienation points. This factor aided to increase reactions kinetics.

This is demonstrated by comparing the hydrogen evolution reaction on the two catalysts. Hydrogen evolution is closely related to the production of the chemisorbed hydrogen. Figure 10 shows that for a given current of 20 mA, generation of chemisorbed hydrogen takes place at more anodic potential with the conducting catalyst. This means that the conduction of the matrix allows a higher number of metallic nanoaggregates to be polarized, which favours an effective presence of chemisorbed hydrogen.

In parallel, because of the importance of the adsorption step of the target molecule, the adsorption properties of the two catalysts towards phenol were compared.

Tests were carried out in the dynamic cell to determine the rate of adsorption of phenol onto Pd/undoped and Pd/F-doped SnO_2 at pH 5 using an initial concentration of 10^{-2} mol L^{-1} (Fig. 11). The concentration of phenol decreased upon contact with the two matrices. Overall, the shapes of phenol rate adsorption are similar on undoped and F-doped SnO_2. This means that the adsorption is similar on the two catalysts, within experimental error.

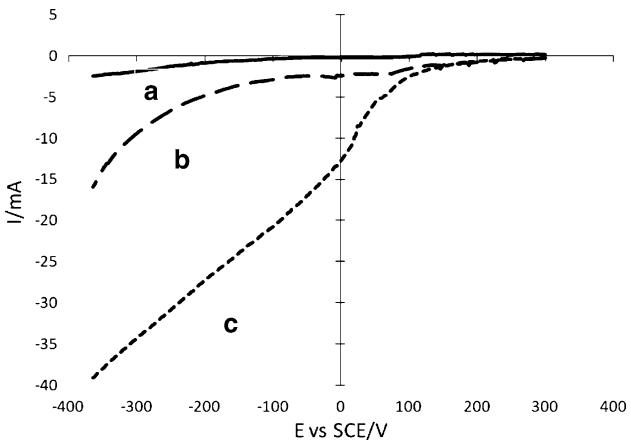

Fig. 10 Linear sweep voltammetry (in acetic buffer 0.5 M, pH 5) for hydrogen evolution on: (**a**) RVC, (**b**) RVC + Pd/undoped SnO_2 400 °C and (**c**) RVC + Pd/F-doped SnO_2 400 °C. Scan rate is 20 mV s^{-1}

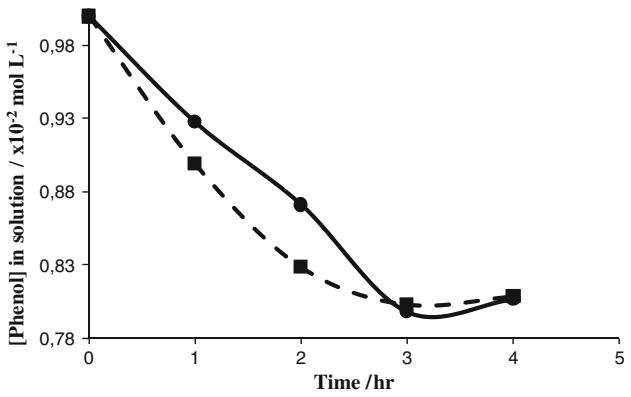

Fig. 11 Rate of adsorption of phenol onto: (■) Pd/undoped and (●) Pd/F-doped SnO_2 powders obtained at 400 °C

Thus, it is clear that the higher efficiency of hydrogenation on the F-doped catalyst is not solely dependent on the adsorption phenomenon; therefore, conductivity strongly influences the efficiency.

It is important to notice that by choosing the right catalyst, the desired product can be obtained. With undoped support catalyst, cyclohexanone is obtained from phenol hydrogenation whereas the doped one principally gives cyclohexanol after 400 C (Figs. 8 and 9). As shown in Table 1, the conductivity changes with calcination temperature. Three catalysts, obtained at different temperatures, were tested in ECH experiments to determine the influence of conductivity. The results are shown in Fig. 12. ECH efficiency depends on the calcination temperature. From 350 to 400 °C, the greatest increase in the electrocatalytic activity was observed. If the catalyst obtained at 350 °C led to the formation of less than 15% of cyclohexanone (first step), with the catalyst obtained at 400 °C 100% of cyclohexanol (final step) was obtained. At 600 °C, the performance decreased drastically, with only 25% of cyclohexanone formation after 400 C were passed. These differences are not due to the phase composition of Pd metallic aggregates apart from the morphology, because, as seen previously, before ECH experiments, 50 C were passed to reduce all PdO to metallic Pd nanoparticles (Fig. 7). This behaviour is therefore linked to the physical and chemical properties of the catalysts, as pointed out by the physical and chemical characterizations. From DRX, MEB and BET analyses, significant structural and morphological changes were noticed with temperature. TGA/DSC and FTIR analyses confirmed chemical modifications in the composition.

One explanation for the weak performance of the catalyst treated at 350 °C seems to be the presence of residual organics and also the absence of conductivity of the matrix. From 400 to 600 °C, the conductivity increased, so an increase in the efficiency was expected; however, a lower performance was obtained from the catalyst treated at 600 °C. Comprehension of this weak catalytic activity at 600 °C comes from the adsorption isotherms of phenol at pH 5 determined after 72 hours contact with the three catalysts (Fig. 13). The adsorption isotherms exhibited linear behavior with the substrate concentration. The catalysts at 350 and 400 °C were practically similar in adsorption, whereas at 600 °C the adsorption was stronger, the amount of uptake being approximately twice that of the other for the same initial concentration beyond a phenol concentration of 4×10^{-3} mol L^{-1}. The comparison between the electrocatalytic hydrogenation and adsorption

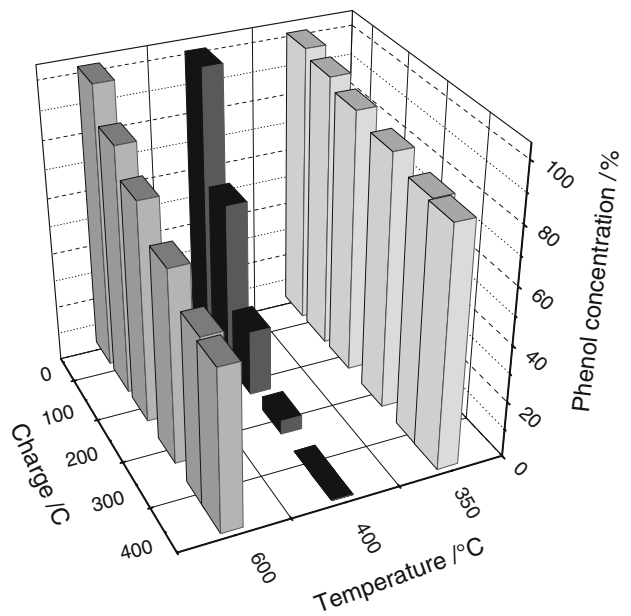

Fig. 12 Remaining fraction of phenol in acetic buffer (0.5 M) at pH 5 as a function of the total charge and the calcination temperature on Pd/F-doped SnO_2 obtained at 350, 400 and 600 °C

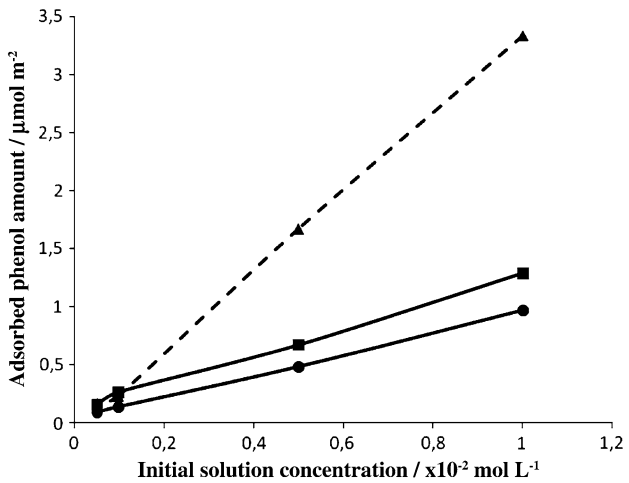

Fig. 13 Adsorption isotherm for phenol after 72 hours contact with Pd/F-doped SnO_2 in acetic buffer (0.5 M) at pH 5: (●) 350 °C, (■) 400 °C and (▲) 600 °C

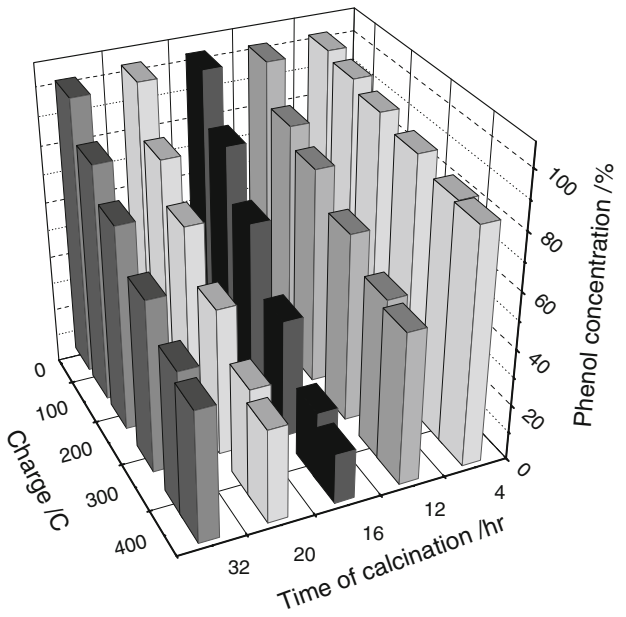

Fig. 14 Remaining fraction of phenol in acetic buffer (0.5 M) at pH 5 as a function of the total charge and the time of calcination on Pd/F-doped SnO_2 obtained at 350 °C, during 4, 12, 16, 20 and 32 h

isotherm experiments clearly indicates that when phenol is adsorbed too strongly (reaction 2) the hydrogenation reaction is inhibited. The same conclusion was drawn by St-Pierre et al [25] in the case of ECH of cyclohexanone, using organic functions to modify the silica surface of the catalyst. This finding shows that ECH efficiency is directly correlated to the relative adsorption of the substrate on the catalyst surface. Thus, the weak performance of the catalyst at 600 °C is explained by the fact that adsorption is a prior step. So, the conductivity effect only contributes when the right adsorption conditions are present.

Figure 14 presents the evolution of ECH efficiency of phenol as a function of calcination time at 350 °C. The time of calcination influences the catalyst performance. The efficiency improves with increased calcination time, the maximum efficiency being obtained around 16 hours. For higher values the performance decreases sharply. As explained previously, the physical and chemical natures of the catalyst change with temperature, and time of calcination seems to play the same role. At 350 °C, during calcination, different crystallization processes occurred, and also removal of residual organics, desorption of the hydroxyl groups and morphological changes. At this temperature the catalysts remained non conductive.

5 Conclusion

SnO_2-based powders were prepared using the sol–gel method. With this technique, it was possible to obtain electrocatalysts with good dispersion of Pd nanoaggregates. A conducting catalyst support was obtained by doping tin dioxide with fluorine. These new electrodes demonstrate the importance of the support.

ECH is highly depending on the physical, chemical and conducting properties of the matrix.

Although the effectiveness depends on the temperature and calcination time, the primary factor governing the ECH process is the adsorption. Conductive powder provides good efficiency due to the simultaneous polarization of all the Pd nanoparticles.

Acknowledgements We thank the "Coopération France-Burkina Faso" for the BGF funding and the University of Sherbrooke for financial and material support.

References

1. Cheng IF, Fernando Q, Korte N (1997) Environ Sci Technol 31:1074
2. Ruest L, Ménard H, Moreau V, Laplante F (2002) Can J Chem 80:1662
3. Dubé P, Kerdouss F, Laplante F, Proulx P, Brossard L, Ménard H (2003) J Appl Electrochem 33:541
4. Mahdavi B, Lafrance A, Martel A, Lessard J, Ménard H (1997) J Appl Electrochem 27:605
5. Kung HH, Brookes BI, Burwell JRL (1974) J Phys Chem 78:875
6. Wismeijer AA, Kieboom APG, Van Bekkum H (1986) Recl Trav Chim Pays-Bas 105:129
7. Casadei MA, Pletcher D (1988) Electrochim Acta 33:117
8. Amouzegar K, Savadogo O (1997) J Appl Electrochem 27:539
9. Dabo P, Cyr A, Lessard J, Brossard L, Ménard H (1999) Can J Chem 77:1225
10. Laplante F, Bouchard NA, Dubé P, Ménard H, Brossard L (2003) Can J Chem 81:1039
11. Dubé P, Brossard L, Ménard H (2002) Can J Chem 80:345
12. Miller LL, Christensen L (1978) J Org Chem 43:2059
13. Misra RA, Sharma BL (1979) Electrochim Acta 24:727
14. Park C, Keane MA (2003) J Colloid Interface Sci 266:183
15. Cirtiu CM, Hassani HO, Bouchard NA, Rowntree PA, Ménard H (2006) Langmuir 22:6414
16. Liberkova K, Touroude R (2002) J Mol Catal A Chem 180:221
17. Rodrigues ECPE, Olivi P (2003) J Phys Chem Solids 64:1105
18. Siciliano P (2000) Sen Actuators B 70:153
19. Esteves MC, Gouvêa D, Sumodjo PTA (2004) Appl Surf Sci 229:24
20. Mahfouz RM, Alshhri SM, Monshi MAS, El-Salam NMAS (2004) Radiat Eff Defects Solid 159:345
21. Rella R, Serra A, Siciliano P, Vasanelli L, De G, Licciulli A (1997) Thin Solid Films 304:339
22. Zhu G, Han J, Zemlyanov DY, Ribeiro FH (2005) J Phys Chem B 109:2331
23. Zhang G, Liu M (1999) J Mat Sci 34:3213
24. Maxted EB, Ali SI (1961) J Chem Soc 83:4137
25. St-Pierre G, Chagnes A, Bouchard NA, Harvey PD, Brossard L, Ménard H (2004) Langmuir 20:6365